JOC Article
pubs.acs.org/joc

Mechanistic Insights on the Magnesium(II) Ion-Activated Reduction of Methyl Benzoylformate with Chelated NADH Peptide β-Lactam Models

Jesus M. Aizpurua,* Claudio Palomo,* Raluca M. Fratila, Pablo Ferrón, Ana Benito, Enrique Gómez-Bengoa, José I. Miranda, and José I. Santos

Departamento de Química Orgánica-I, Universidad del País Vasco, Joxe Mari Korta R&D Center. Avda, Tolosa-72, 20018 San Sebastián, Spain

jesusmaria.aizpurua@ehu.es

Received June 11, 2009

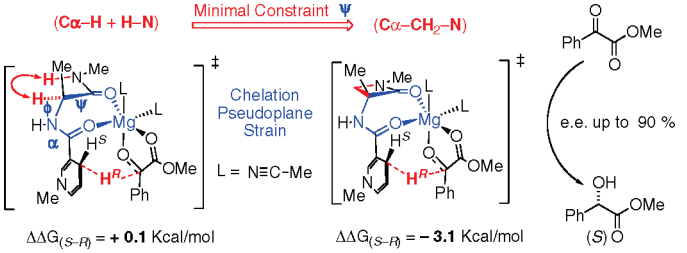

Mechanistic details of the Mg^{2+} ion-activated enantioselective reduction of methyl benzoylformate have been investigated at a B3LYP/6-31G* theory level, using peptide NADH models **1** rigidified with a β-lactam ring. Computation of the reaction pathway revealed important structural differences between the intermediate NADH/Mg^{2+}/$ArCOCO_2R$ ternary complexes **3** and the corresponding transition states leading to enantiomeric methyl mandelates. Thus, ternary complexes showed the dihydronicotinamide moiety placed quasiequatorial to a seven-membered chelation pseudoplane including the two amide carbonyls and the Mg^{2+} cation, whereas productive transition states were strongly deformed with the dihydronicotinamide group oriented quasiaxial to the chelation pseudoplane. This chelation model was further applied to acyclic nonrigidified NADH models and, based on the fluxional mobility of the peptide chain bonds, experimental enantioselectivities were correctly predicted. Parallel experiments were also conducted in deuterated acetonitrile, using NMR techniques, to study the structure of the binary complexes **2** (NADH/Mg^{2+}) and ternary complexes **3** (NADH/Mg^{2+}/$PhCOCO_2Me$). Finally, owing to the incorporation of two diastereotopic trimethylsilyl NMR-tags in the β-lactam-NADH peptidomimetics, a nonproductive ternary complex predicted by calculations could be observed and its structure characterized on the basis of ROESY experiments and molecular modeling.

Introduction

The nicotinamide adenine dinucleotide phosphate NAD(P)H/$NAD(P)^+$ redox system is of major importance for several biological processes such as photosynthesis, glycolysis, fatty acid synthesis, citric acid cycle, and amino acid metabolism. Many organic and bioorganic chemists have been challenged to mimic this type of biochemical reaction, and since Ohno and co-workers[1] reported the first Mg^{2+}-assisted asymmetric reduction of alkyl benzoylformates with a chiral coenzyme NADH model **1** (Scheme 1), a large number of such compounds have been described.[2] Various strategies have also been developed to achieve directional and orientational control in these redox reactions. Among the more successful, the use of inherently chiral 4-methyl-1,4-dihydropyridines **1**-(I)[3] or

(1) (a) Ohnishi, Y.; Numakunai, M.; Ohno, A. *Tetrahedron Lett.* **1975**, 3183–3184. (b) Ohnishi, Y.; Kagami, M.; Ohno, A. *J. Am. Chem. Soc.* **1975**, *97*, 4766–4768.

(2) Reviews on NADH models: (a) Burgess, V. A.; Davies, S. G.; Skerlj, R. T. *Tetrahedron: Asymmetry* **1991**, *2*, 299–328. (b) Dupas, G.; Levacher, V.; Bourguignon, J.; Quéguiner, G. *Heterocycles* **1994**, *39*, 405–429. (c) Wang, N. X.; Zhao, J. *Synlett* **2007**, 2785–2791.

(3) (a) Ohno, A.; Ikeguchi, M.; Kimura, T.; Oka, S. *J. Chem. Soc., Chem. Commun.* **1978**, 328–329. (b) De Kok, P. M.; Bastiaansen, L. A.; van Lier, P. M.; Vekemans, J. A.; Buck, H. M. *J. Org. Chem.* **1989**, *54*, 1313–1320.

DOI: 10.1021/jo901236d Published on Web 07/31/2009

SCHEME 1. General Pathway for the Reduction of Alkyl Benzoylformates with Chiral NADH Models 1 in the Presence of Magnesium Cation

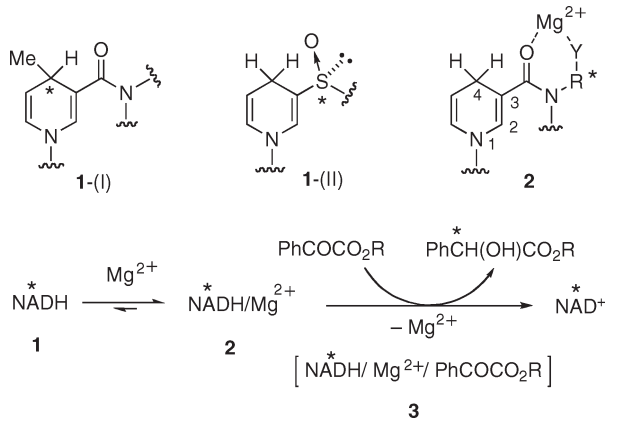

3-sulfinyl-1,4-dihydropyridines **1**-(II)[4] can be mentioned. However, chelation control through bidentate models **2**, retaining the original 1,4-dihydronicotinamide and including some ancillary Mg^{2+}-coordinating groups (e.g., C=O, OH), remains the closest artificial system to mimic the enzymatic chiral field of biological NADH reductions.[5]

The general reaction mechanism (Scheme 1) is assumed to involve the coordination of chiral NADH models **1** with magnesium ion to afford complexes **2**, which are the actual reducing agents of alkyl benzoylformates through the unstable ternary entities **3**.[1a,2b] The NADH/Mg^{2+}/$PhCOCO_2R$ entities formed from chelated NADH models **2** are often defined indistinctly as "transient ternary complexes" or "transition states" and are assumed to govern the enantioselectivity of the hydrogen transfer step. However, despite the excellent enantiomeric excesses attained in many instances, the structural reasons invoked to explain the sense of the facial discrimination remain vague and purely empirical (Figure 1).

For example, (a) the coordination geometry of magnesium ion varies from tetrahedral to octahedral, (b) the complexation sites of NADH models seldom include the nitrogen atom of the dihydropyridine ring[5] or peptide carbonyls,[6,7] (c) the benzoylformate ketoester moiety is represented interacting with the magnesium cation either in a *s*-trans conformation[8] or in a chelated *s*-cis conformation[7,9] and, (d) most models include a carbonyl-activating interaction of the magnesium cation with the ketone group of alkyl benzoylformates, in line with the mechanism accepted for alcohol dehydrogenase enzymes.[10] Indeed, it is generally assumed that most of the deformations found in the enzyme-bonded 1,4-dihydronicotinamide moiety can be translated to the enzyme-free NADH/Mg^{2+}/$PhCOCO_2R$ models from the ternary complexes formed by NADH coenzyme, Zn^{2+}-containing L-lactate dehydrogenase enzyme and pyruvate substrate. According to X-ray analysis[10b] the enzyme-bound carboxamide group is about 30° out-of-plane with respect to the dihydropyridine ring. In addition, extensive theoretical calculations[11] suggest

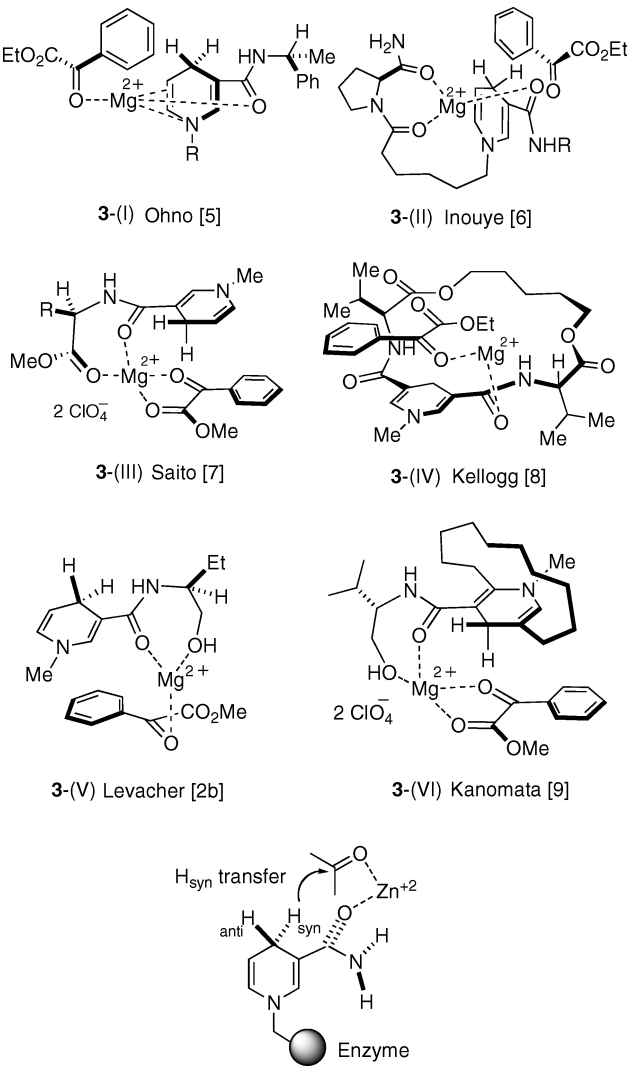

FIGURE 1. Original drafts of ternary entities **3**-(I−VI) proposed by several authors to explain the facial discrimination observed for the reduction of alkyl benzoylformates with chelated chiral NADH models. "H*syn* rule" (bottom): the carboxamide C=O group and the transferring hydrogen are *syn*-oriented in the enzymatic transition states.

(4) (a) Imanishi, T.; Hamano, Y.; Yoshikawa, H.; Iwata, C. *J. Chem. Soc., Chem. Commun.* **1988**, 473–475. (b) Obika, S.; Nishiyama, T.; Tatematsu, S.; Miyashita, K.; Imanishi, T. *Tetrahedron* **1997**, *53*, 3073–3082. (c) Li, J.; Liu, Y. C.; Deng, J. G. *Tetrahedron: Asymmetry* **1999**, *10*, 4343–4347. (d) Li, J.; Liu, Y. C.; Deng, J. G.; Li, X. Z.; Cui, X.; Li, Z. *Tetrahedron: Asymmetry* **2000**, *11*, 2677–2682.

(5) Ohno, A.; Kimura, T.; Yamamoto, H.; Kim, S. G.; Oka, S.; Ohnishi, Y. *Bull. Chem. Soc. Jpn.* **1977**, *50*, 1535–1538.

(6) For previous conformationally restricted NADH peptides, see: (a) Baba, N.; Oda, J.; Inouye, Y. *J. Chem. Soc., Chem. Commun.* **1980**, 815–817. (b) Seki, M.; Baba, N.; Oda, J.; Inouye, Y. *J. Am. Chem. Soc.* **1981**, *103*, 4613–4615. (c) Seki, M.; Baba, N.; Oda, J.; Inouye, Y. *J. Org. Chem.* **1983**, *48*, 1370–1373.

(7) Saito, R.; Naruse, S.; Takano, K.; Fukuda, K.; Katoh, A.; Inouye, I. *Org. Lett.* **2006**, *8*, 2067–2070.

(8) Talma, A. J.; Jouin, P.; De Vries, J. G.; Trootswijk, C. B.; Werumeus Buning, G. H.; Waninge, J. K.; Visscher, J.; Kellogg, R. M. *J. Am. Chem. Soc.* **1985**, *107*, 3981–3997.

(9) (a) Kanomata, N.; Nakata, T. *Angew. Chem., Int. Ed. Engl.* **1997**, *36*, 1207–1211. (b) Kanomata, N.; Nakata, T. *J. Am. Chem. Soc.* **2000**, *122*, 4563–4568.

(10) (a) Eklund, H.; Branden, C. I. In *Biological Macromolecules and Assemblies*; Wiley: New York, 1985. (b) Eklund, H.; Samama, J. P.; Jones, T. A. *Biochemistry* **1984**, *33*, 5982–5996.

(11) According to the original Benner's model, this phenomenon would be caused by a "reverse anomeric effect" that is unlikely to occur in 1,4-dihydronicotinamides without *N*-glycosidic groups, see: (a) Nambiar, P. K.; Stauffer, D. M.; Kolodziej, P. A.; Benner, S. A. *J. Am. Chem. Soc.* **1983**, *105*, 5886–5890. (b) Wu, Y. D.; Houk, K. N. *J. Am. Chem. Soc.* **1991**, *113*, 2353–2358. (c) Almarsson, O.; Bruice, T. C. *J. Am. Chem. Soc.* **1993**, *115*, 2125–2138. (d) Luo, J.; Bruice, T. C. *J. Am. Chem. Soc.* **2001**, *123*, 11952–11959.

that the 1,4-dihydropyridine ring adopts a flat boat conformation in the enzymatic process, facilitating the stereospecific transfer of the pseudoaxial C^4-H hydride placed in a *syn* disposition with respect to the carboxamide C=O. This "H*syn* transfer rule" is generally accepted to be at the origin of the facial discrimination and subsequent enantioselectivity in the nonenzymatic reduction of alkyl benzoylformates with $NADH/Mg^{2+}$ systems.[12]

Unfortunately, most of the structures **3**-(I) to **3**-(VI) used to describe enzyme-free ternary entities from chelated chiral NADH models are approximative drafts rather than actual molecular modeling structures. As a matter of fact, no accurate ab initio computational study has been reported yet detailing the structures and relative stabilities of the Mg^{2+}-centered ternary complexes and the transition states that account for the experimental enantioselectivities attained in NADH model-based nonenzymatic reductions.[13]

Considerable efforts have also been devoted to provide spectroscopic evidence for the structural elucidation of the intermediates involved in the enzyme-free enantioselective reduction of α-keto esters with chiral NADH models. For example, the complexation between metal ions and several NADH models to form the rather stable binary complexes **2** has been extensively investigated with use of NMR, UV, IR, and fluorescence techniques[2b,8,14] and the structural features of some of them have been established in detail. In contrast, the very few examples in the literature so far dealing with the direct detection of ternary entities **3**[15] concern only achiral NADH mimetics.

We present herein a detailed computational model to explain the enantioselective reduction of methyl benzoylformate with peptide-containing NADH mimetics under nonenzymatic conditions. The proposed model is based on the combination of two structural features: first, the chelation of NADH peptides with Mg^{2+} cation to form a seven-membered ring (Figure 2), and second, the application of the Freidinger's lactam peptidomimetic[16] approach to promote

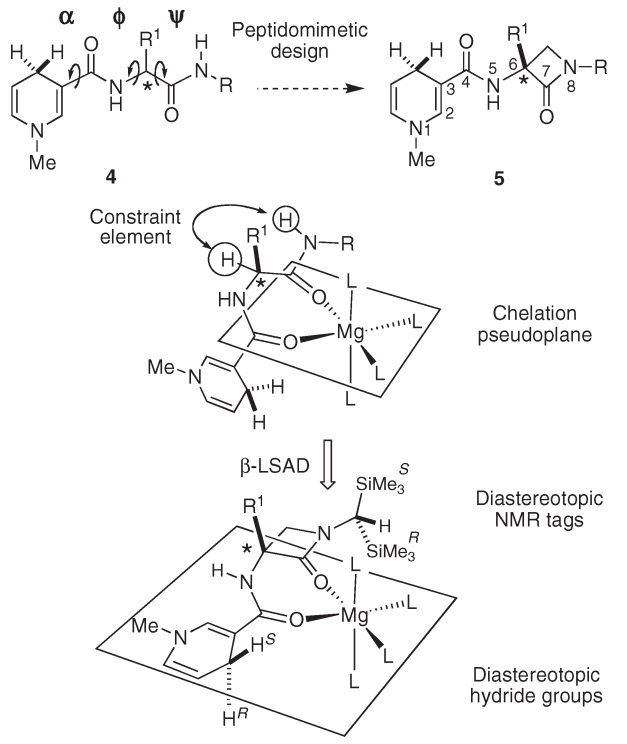

FIGURE 2. The "*β*-Lactam Scaffold-Assisted Design" (*β*-LSAD) approach to NADH models: formal insertion in the native peptide of a carbon atom ($C\alpha-H + H-N \rightarrow C\alpha-CH_2-N$) provides pseudopeptides **5** rigidified around the ψ ($\approx 120°$) torsion angle. Definition of dihedral angles: α, ($C^2-C^3-C^4-N^5$); ϕ, ($C^4-N^5-C^6-C^7$); and ψ, ($N^5-C^6-C^7-N^8$).

the covalent rigidification of the amide linkage in NADH peptide ligands. In particular, using specially designed chiral *β*-lactam NADH models that favor stereodifferentiation with respect to the corresponding open peptides, we have conducted a combined experimental and DFT computational study that has allowed us to establish for the first time the quantification of the relative stabilities and structural characteristics of the chelated ternary complexes peptide-$NADH/Mg^{2+}/PhCOCO_2Me$ and the transition states thereof. Furthermore, incorporation of diastereotopic silyl tags in these *β*-lactam NADH models has permitted the detection of a $NADH/Mg^{2+}/PhCOCO_2Me$ ternary complex with NMR spectroscopy techniques.

Results and Discussion

NADH Model Design. Among the diverse families of NADH models, nicotinamide peptides **4**[17] (Figure 2) are known to represent the closest imitation of the enzyme/coenzyme complex and were expected to provide valuable information concerning the NADH/substrate/coenzyme interaction. From a structural viewpoint, they are also expected to arrange around the Mg^{2+} cation in a doubly coordinated fashion within a seven-membered chelation pseudoplane. However, NADH peptides **4** could still enjoy considerable conformational freedom because of the rotations

(12) Vasse, J. L.; Levacher, V.; Bourguignon, J.; Dupas, G. *Tetrahedron: Asymmetry* **2002**, *13*, 227–232.

(13) For a semiempirical (MNDO-PM3) study of the Mg^{2+}-mediated reduction of methyl benzoylformate with achiral dihydronicotinamide, see: (a) Toyooka, Y.; Matsuzawa, T.; Eguchi, T.; Kakinuma, K. *Tetrahedron* **1995**, *51*, 6459–6474. For theoretical studies on conformational features of NADH analogues, see: (b) Donkersloot, M. C. A.; Buck, H. M. *J. Am. Chem. Soc.* **1981**, *103*, 6554–6558. (c) Brewster, M. E.; Pop, E.; Huang, M.-J.; Bodor, N. *Heterocycles* **1994**, *37*, 1373–1415. (d) Okamura, M.; Mikata, Y.; Yamazaki, N.; Tsutsumi, A.; Ohno, A. *Bull. Chem. Soc. Jpn.* **1993**, *66*, 1197–1203. (e) Obika, S.; Nishiyama, T.; Tatematsu, S.; Miyashita, K.; Imanishi, T. *Tetrahedron* **1997**, *53*, 3073–3082. (f) De Luca, G.; Marino, T.; Mineva, T.; Russo, N.; Toscano, M. *J. Mol. Struct. (THEOCHEM)* **2000**, *501−502*, 215–220. (g) Zhong, H.; Bowen, J. P. *J. Mod. Graph. Model.* **2005**, *24*, 1–9.

(14) (a) Hughes, M.; Prince, R. H. *J. Inorg. Nucl. Chem.* **1978**, *40*, 703–712. (b) De Kok, P. M. T.; Donkersloot, M. C. A.; van Lier, P. M.; Meulendijks, G. H. W. M.; Bastiaansen, L. A. M.; van Hooff, H. J. G.; Kanters, J. A.; Buck, H. M. *Tetrahedron* **1986**, *42*, 941–959. (c) Zehani, S.; Lin, J.; Gelbard, G. *Tetrahedron* **1989**, *45*, 733–740. (d) Tamagaki, S.; Simojo, Y.; Mimura, T.; Tagaki, W. *Bull. Chem. Soc. Jpn.* **1989**, *62*, 1593–1600. (e) Wu, Y. D.; Houk, K. N. *J. Org. Chem.* **1993**, *58*, 2043–2045. (f) Bédat, J.; Plé, N.; Dupas, G.; Bourguignon, J.; Quéguiner, G. *Tetrahedron: Asymmetry* **1995**, *6*, 923–932. (g) Leroy, C.; Levacher, V.; Dupas, G.; Quéguiner, G.; Bourguignon, J. *Tetrahedron: Asymmetry* **1997**, *8*, 3309–3318. (h) Vitry, C.; Bédat, J.; Prigent, Y.; Levacher, V.; Dupas, G.; Salliot, I.; Quéguiner, G.; Bourguignon, J. *Tetrahedron* **2001**, *57*, 9101–9108.

(15) (a) Fukuzumi, S.; Nishizawa, N.; Tanaka, T. *Chem. Lett.* **1983**, 1755–1758. (b) Ohno, A.; Yamamoto, H.; Oka, S. *Bull. Chem. Soc. Jpn.* **1981**, 3489–3491.

(16) (a) Freidinger, R. M.; Veber, D. F.; Perlow, D. S.; Brookas, J. R.; Saperstein, R. *Science* **1980**, *210*, 656–658. (b) Freidinger, R. M. *J. Med. Chem.* **2003**, *46*, 5553–5566.

(17) For extended NADH peptide models, see: (a) Endo, T.; Hayashi, Y.; Okawara, M. *Chem. Lett.* **1977**, 391–394. (b) Endo, T.; Kawasaki, H.; Okawara, M. *Tetrahedron. Lett.* **1979**, 23–26. (c) Saito, R.; Naruse, S.; Takano, K.; Fukuda, K.; Katoh, A.; Inouye, I. *Org. Lett.* **2006**, *8*, 2067–2070.

TABLE 1. Preparation of NADH β-Lactam Peptidomimetics 5a−f and 8

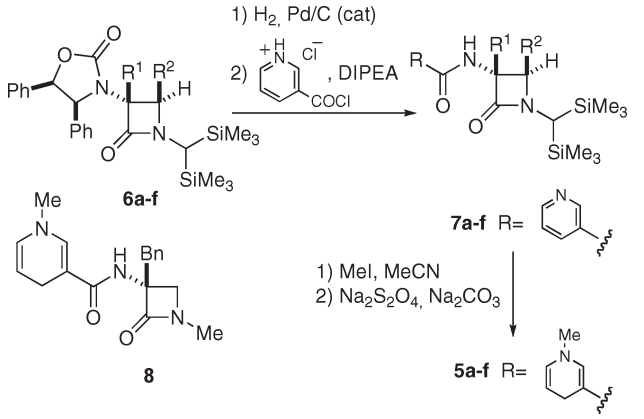

R^1	R^2	Product	Yield [%][a]	Product	Yield [%][b]
Me	H	**7a**	64	**5a**	84
Bn	H	**7b**	85	**5b**	64
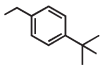	H	**7c**	60	**5c**	57
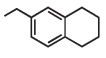	H	**7d**	59	**5d**	65
Bn	*i*Bu	**7e**	66	**5e**	87
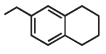	*i*Bu	**7f**	71	**5f**	58

[a]Overall yield from **6a**−**f**. [b]Overall yield from **7a**−**f**.

around α, ϕ, and ψ torsion angles within the 1,4-dihydronicotinamide and the α-amino acid peptide chain. In a seminal work, Inouye demonstrated that the enantiomeric excess of the mandelate reduction products can be enhanced by incorporating the torsionally blocked proline amino acid into the NADH peptide models.[6] We reasoned that the incorporation of a planar constraint by means of a lactam mimetic might reduce the flexibility around the chelation pseudoplane, thus enabling a more accurate interpretation of computational calculations (by minimizing the energy contribution due to conformational mobility, see below) and facilitating the interpretation of interproton NOE interactions in NMR experiments. To this end, we selected the minimal-sized and puckering-free β-lactams **5** designed according to the "β-LSAD" principle (see Figure 2).[18] This constraint fixed the ψ angle to ~120°, strongly limiting the rotation around ϕ. In addition, NMR-tagging could be easily accomplished by placing two diastereotopic trimethylsilyl groups [R = $CH(SiMe_3)_2$] internally oriented toward each face of the chelation pseudoplane.

(18) (a) Palomo, C.; Aizpurua, J. M.; Benito, A.; Miranda, J. I.; Fratila, R. M.; Matute, C.; Domercq, M.; Gago, F.; Martín-Santamaria, S.; Linden, A. *J. Am. Chem. Soc.* **2003**, *125*, 16243–16260. (b) Palomo, C.; Aizpurua, J. M.; Balentova, E.; Jimenez, A.; Oyarbide, J.; Fratila, R. M.; Miranda, J. I. *Org. Lett.* **2007**, *9*, 101–104.

TABLE 2. Asymmetric Reduction of Methyl Benzoylformate with NADH Models 5a−e and 8

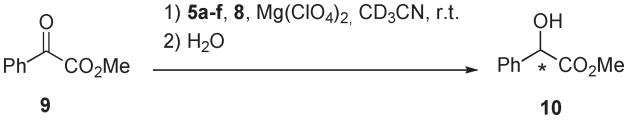

entry	NADH model	reaction time [h][a]	yield [%][b]	ee [%][c]	major enantiomer
1	**5a**	16	95	73	*S*
2	**5b**	16	66	78	*S*
3	**5c**	18	>99	82	*S*
4	**5d**	18	>99	90	*S*
5	**5e**	16	49	90	*S*
6	**5f**	18	94	90	*S*
7	**8**	16	60	60	*S*

[a]Reactions were quenched with water when complete consumption of the model NADH was observed by ^{1}H NMR. [b]Calculated on the basis of model NAD^+ formation. [c]Determined by HPLC, using the Chiralcel OD stationary phase.

Synthesis of β-Lactam NADH Peptidomimetics and Biomimetic Reduction of Methyl Benzoylformate. On the basis of the previous work from our laboratory, the synthesis of NADH β-lactam peptidomimetics **5** (Table 1) was addressed starting from the readily available enantiopure *N*-[bis-(trimethylsilyl)methyl]-β-lactams **6a**−**f**.[19] Hydrogenolytic cleavage of the oxazolidinone moiety afforded the corresponding α-amino-β-lactams[20] which were next coupled with nicotinyl chloride hydrochloride in the presence of diisopropylethylamine (DIPEA) to give the corresponding nicotinamide derivatives **7a**−**f**. Quaternization of the pyridine nitrogen atom with methyl iodide and subsequent regioselective reduction with sodium dithionite provided the desired NADH models **5a**−**f**. Interestingly, this methodology also permitted the incorporation of a second β-substituent in the azetidinone ring to afford the α,β-disubstituted models **5e**−**f**. Finally NADH peptidomimetic **8**, the desilylated analogue of model **5b**, was prepared similarly from **7b** after desilylation with tetrabutylammonium fluoride in THF at reflux in 64% isolated yield (for full experimental details, see the Supporting Information).

Enantioselective reduction of methyl benzoylformate **9** with the NADH models was investigated in the presence of magnesium perchlorate in acetonitrile at room temperature, and the results obtained are summarized in Table 2. A uniform stereoinduction tendency was observed in all instances affording the *S*-(+) enantiomer of methyl mandelate **10** as the major reaction product. The enantiomeric excess was increased by bulkier α-substituents or cis-α,β-disubstitution on the azetidinone ring. Finally, in an experiment conducted to rule out any particular stereodirecting bias arising from the bis(trimethylsilyl)methyl group, the desilylated model **8** was also tested for reduction, providing

(19) (a) Palomo, C.; Aizpurua, J. M.; Legido, M.; Galarza, R.; Deya, P. M.; Dunogues, J.; Picard, J. P.; Ricci, A.; Seconi, G. *Angew. Chem., Int. Ed. Engl.* **1996**, *35*, 1239–1241. (b) Palomo, C.; Aizpurua, J. M.; Legido, M.; Mielgo, A.; Galarza, R. *Chem. Eur. J.* **1997**, *3*, 1432–1441. (c) Palomo, C.; Aizpurua, J. M.; Ganboa, I.; Benito, A.; Cuerdo, L.; Fratila, R. M.; Jimenez, A.; Loinaz, I.; Miranda, J. I.; Pytlewska, K. R.; Micle, A.; Linden, A. *Org. Lett.* **2004**, *6*, 4443–4446.

(20) In the case of α-(2-methylnaphthyl)-β-lactams **6d** and **6f** a partial hydrogenation of the naphthalene moiety was observed and the corresponding 5,6,7,8-tetrahydronaphthyl derivatives were obtained.

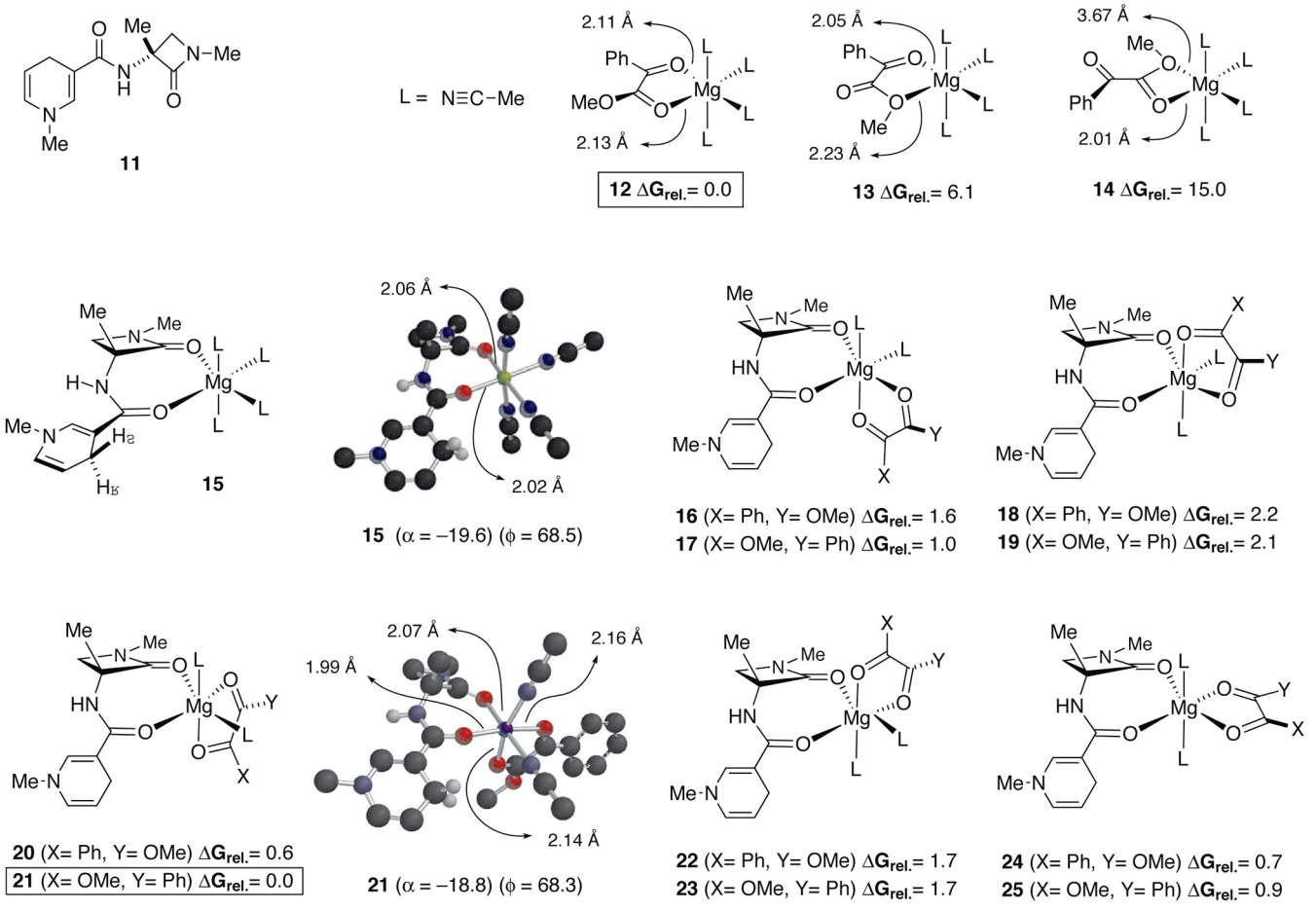

FIGURE 3. Binary and ternary complexes of octahedral Mg^{2+} with methyl benzoylformate **9** and NADH β-lactam model **11** in acetonitrile. Relative free energy values are in kcal/mol. B3LYP/6-31G*-optimized geometries of binary complex **15** and ternary complex **21** are shown omitting all the hydrogen atoms, except the amide NH and the NADH methylene. Dihedral angles as defined in Figure 2.

the (*S*)-methyl mandelate in slightly lower enantiomeric excess than its silylated β-lactam counterpart **5b** (compare entries 2 and 7).

Computational Analysis. To study the reaction mechanism and to ascertain the origin of the stereoselectivity observed for the reduction of methyl benzoylformate **9** with NADH β-lactam peptidomimetics **5**, we selected first the model structure **11** (Figure 3). The flexible benzylic moieties in compounds **5a**−**f** and the bulky $CH(SiMe_3)_2$ were replaced by the less demanding and more rigid two methyl groups to shorten the computational time and limit the conformational energy. For the initial model, all structures were optimized by using the density functional B3LYP[21] and the 6-31G* basis sets as implemented in Gaussian 03.[22] All energy minima and transition structures were characterized by frequency analysis. The energies reported in this work include zero-point vibrational energy corrections (ZPVE) and are not scaled. The intrinsic reaction coordinates (IRC)[23] were followed to verify the energy profiles connecting each transition structure to the correct associated local minima. Single-point calculations with the self-consistent reaction field (SCRF) based on the IEF-PCM[24] solvation model (MeCN, ε = 36.64) were carried out at the B3LYP/6-311++G** level on the previously optimized transition states and stationary points.

The relative free energies at 298 K and some representative structural parameters of the divalent cationic binary complexes **12**−**15** and the ternary complexes **16**−**25** are summarized in Figure 3. They were formally built up from the magnesium complex $[Mg(NCMe)_6]^{2+}$ by displacement of two or four acetonitrile ligands with methyl benzoylformate **9** and/or the β-lactam NADH model **11**. In all cases, the bonding patterns were created assuming an octahedral coordination geometry for the Mg^{2+} cation.[25]

The formation of the binary complexes $[Mg(NCMe)_4/PhCOCO_2Me]^{2+}$ showed Gibbs free energies of −20.6 (**12**), −14.5 (**13**), and −5.6 kcal/mol (**14**), respectively. Five-membered cyclic structure **12**, chelating together the magne-

(21) (a) Lee, C.; Yang, W.; Parr, R. G. *Phys. Rev. B* **1988**, *37*, 785–789. (b) Becke, A. D. *J. Chem. Phys.* **1993**, *98*, 5648–5652. (c) Kohn, W.; Becke, A. D.; Parr, R. G. *J. Phys. Chem.* **1996**, *100*, 12974–12980.

(22) Frisch, M. J.; et al. *Gaussian 03*, Revision D.03; Gaussian, Inc., Wallingford, CT, 2004.

(23) Gonzalez, C.; Schlegel, H. B. *J. Phys. Chem.* **1990**, *94*, 5523–5527.

(24) (a) Cancès, E.; Mennucci, B.; Tomasi, J. *J. Chem. Phys.* **1997**, *107*, 3032–3047. (b) Cossi, M.; Barone, V.; Mennuci, B.; Tomasi *J. Chem. Phys. Lett.* **1998**, *286*, 253–260. (c) Tomasi, J.; Mennucci, B.; Cancès, E. *J. Mol. Struct.* (*THEOCHEM*) **1999**, *464*, 211–226.

(25) (a) Kluge, S.; Weston, J. *Biochemistry* **2005**, *44*, 4877–4885. (b) At low concentration of $Mg(ClO_4)_2$ in acetonitrile most of the six coordination sites of Mg are filled with CD_3CN, whereas at high concentration one or more sites are more likely filled with the ClO_4^- counterions, see: Cha, J. N.; Cheong, B. S.; Cho, H. G. *J. Phys. Chem. A* **2001**, *105*, 1789–1796.

TABLE 3. Relative Energies (in kcal/mol) and Main Torsion Angles (deg) of the Transition Structures 26−33 Computed at the B3LYP/6-31G* Level for NADH Peptide Mimetics 11 and 11A

entry	NADH	TS	topology[a]	config. **9**	complex	$\Delta G^{\ddagger b,c}$	$0\Delta\Delta G^{\ddagger}$	$\Delta H^{\ddagger b,c}$	α^{d}	ϕ^{d}	ψ^{d}
1	**11**	**26**	(H^R-*re*)	(*S*)	**16**	22.4 (23.0) [16.0][e]	0.0 [0.0][e]	19.3 (20.2)	23.1 (*syn*)	62.0	116.5
2	**11**	**27**	(H^S-*re*)	(*S*)	**16**	25.9 (26.5)	3.5	23.8 (24.8)	−87.3 (*s-clinal*)	60.2	115.7
3	**11**	**28**	(H^R-*si*)	(*R*)	**17**	28.2 (28.2)	5.8	22.4 (24.0)	10.7 (*syn*)	58.7	115.7
4	**11**	**29**	(H^S-*si*)	(*R*)	**17**	31.3 (31.3)	8.9	27.1 (28.7)	−143.3 (*anti*)	62.9	119.3
5	**11**	**30**	(H^R-*si*)	(*R*)	**18**	26.6 (27.8)	4.2	25.0 (25.0)	132.0 (*anti*)	4.3	122.3
6	**11**	**31**	(H^S-*si*)	(*R*)	**18**	25.5 (26.7) [19.7][e]	3.1 [3.7][e]	23.4 (23.4)	−20.9 (*syn*)	−10.7	126.7
7	**11**	**32**	(H^R-*re*)	(*S*)	**19**	28.5 (29.5)	6.1	26.4 (26.8)	149.5 (*anti*)	−11.9	125.3
8	**11**	**33**	(H^S-*re*)	(*S*)	**19**	26.8 (27.8)	5.4	25.6 (26.1)	19.6 (*syn*)	1.4	121.9
9	**11A**	**26A**	(H^R-*re*)	(*S*)	**16A**	20.3 (21.7) [12.5][e]	0.1 [0.0][e]	15.8 (18.0)	22.4 (*syn*)	68.4	139.5
10	**11A**	**27A**	(H^S-*re*)	(*S*)	**16A**	24.5 (25.9)	4.3	21.6 (23.7)	−94.0 (*s-clinal*)	70.0	124.4
11	**11A**	**28A**	(H^R-*si*)	(*R*)	**17A**	24.8 (27.2)	4.6	24.7 (24.7)	−5.9 (*syn*)	70.6	130.5
12	**11A**	**29A**	(H^S-*si*)	(*R*)	**17A**	27.1 (29.5)	6.9	26.3 (26.3)	−149.8 (*anti*)	69.2	154.0
13	**11A**	**30A**	(H^R-*si*)	(*R*)	**18A**	27.5 (27.8)	7.4	25.0 (25.3)	131.2 (*anti*)	−25.1	143.5
14	**11A**	**31A**	(H^S-*si*)	(*R*)	**18A**	20.2 (20.4) [13.0][e]	0.0 [0.5][e]	15.7 (16.0)	−21.6 (*syn*)	−79.6	−128.0
15	**11A**	**32A**	(H^R-*re*)	(*S*)	**19A**	25.9 (25.9)	5.7	21.8 (22.3)	−179.5 (*anti*)	−132.7	−150.0
16	**11A**	**33A**	(H^S-*re*)	(*S*)	**19A**	26.3 (26.3)	6.1	23.5 (22.9)	−1.9 (*syn*)	−79.5	−119.4

[a]Face-selective interaction between the 1,4-dihydronicotinamide (hydride donor) and methyl benzoylformate **9** (hydride acceptor). [b]Activation energies calculated from the ternary complexes **16**−**19**. [c]Values in parentheses correspond to the activation energies calculated from the most stable "productive" ternary structure **17** (entries 1−8) and **19A** (entries 9−16). [d]Dihedral angles as defined in Figure 2. [e]Activation energies from single-point calculation at the B3LYP/6-311++G** level including the IEF-PCM solvation model (MeCN, $\varepsilon = 36.64$).

sium cation with the methyl benzoylformate ketone and the ester carbonyl, was found to be the one conformationally preferred among the bidentate complexes **12**−**14**. This *s*-cis conformation was 6 kcal/mol more stable than the *s*-trans isomer **13** and 15 kcal/mol more stable than the ester-bound isomer **14**. Most of the computed Mg---O=C distances (2.01−2.23 Å) were within the expected range for this kind of coordinated bond, except the Mg---OMe distance in **14** (3.67 Å), which was too long to be considered a dative covalent bond.

The formation of the binary complex **15** was energetically very favored, with a Gibbs free energy of −46.9 kcal/mol for the exchange equilibrium (**11** + $[Mg(NCMe)_6]^{2+} \rightarrow$ $[\mathbf{15}]^{2+}$ + 2 NCMe). This complex included two Mg---O=C bonds which were almost identical in length (2.02 and 2.06 Å). It also comprised a slightly distorted chelation pseudoplane bearing a 1,4-dihydronicotinamide group oriented in a quasiequatorial disposition. The planarity of the seven-membered chelation pseudoplane in complex **15** could be gauged from the dihedral angle ϕ (68.5) encompassing the four central $C^4-N^5-C^6-C^7$ atoms from the fiducial dihydropyridine ring. The *syn* disposition of the 1,4-dihydronicotinamide moiety could also be confirmed from the dihedral angle α (−19.6) within the $C^2-C^3-C^4-N^5$ bonds (see Figure 3). As mentioned above, the methyl benzoylformate molecule formed a strongly preferred *s*-cis chelate with Mg^{2+} in the binary complex **12** and, consequently, this ligand conformation was retained to build up the ternary structures **16**−**25** comprising all ten possible molecular arrangements of **9** around **15**. After B3LYP/6-31G* optimization, small energy differences (only up to 2.2 kcal/mol) were computed between the most stable and the less stable optimized complexes. Accordingly, structures **20** and **21** with the methyl benzoylformate ligand **9** placed in the rear bottom quadrant position were found to be slightly more stable than, say, the isomers **18** and **19** with the methyl benzoylformate ligand placed in the front top quadrant. Moreover, the $\Delta G°$ of the exchange equilibrium from the binary complex **15** to the most stable ternary structure **21** ($[\mathbf{15}]^{2+} + \mathbf{9} \rightarrow [\mathbf{21}]^{2+} + 2NCMe$) was only −5.3 kcal/mol at 25 °C, suggesting the potential for equilibrium between the different ternary complexes at such temperature. The structural parameters of the ternary complexes **16**−**25** were also remarkably homogeneous. For example, the computed Mg---O=C distances ranged in the interval 2.05 ± 0.02 Å for the β-lactam carbonyl; 2.01 ± 0.02 Å for the 1,4-dihydronicotinamide carbonyl; 2.14 ± 0.01 Å for the ketone; and 2.16 ± 0.01 Å for the ester carbonyl. Dihedral angles ϕ varied from 61.8° in complex **17** to 69.8° in complex 25 and, similarly, dihedral angles α were all close to ±20° (*syn*), lying from −18.8° in complex **21** to 12.7° in complex **16** (see the Supporting Information for details). As a consequence, according to these calculations, the seven-membered chelation pseudoplane of the binary complex **15** experienced a practically negligible structural change after the methyl benzoylformate ligand was incorporated to form the ternary complexes **16**−**25**.

Next, an extensive computational survey of the intramolecular hydride transfer reaction step was undertaken with the aim to characterize the possible transition states arising from the ten ternary complexes **16**−**25**. Although the precise mechanism of this step is still controversial and one-electron transfer may occur in some NADH models,[26] a concerted hydride transfer mechanism was considered by analogy with the Hantzsch 1,4-dihydropyridine mechanism described by Simon and Goodman.[27] Not surprisingly, using the β-lactam NADH model **11** only the four complexes **16**−**19** led to canonical transition structures (TS-**26**−**33**, Table 3, entries 1−8), whereas complexes **20**−**25** presented distances between the dihydronicotinamide diastereotopic hydrogens (H^R, H^S) and the methyl benzoylformate ketone carbon atom which were too long to attain potentially "productive" transition states. It was also found that two different reaction topologies were possible for the hydrogen transfer in each ternary complex **16**−**19**, yielding a total of 8 transition states (for detailed structures, see the Supporting Information). Nonetheless, as the configuration of the final product was dictated solely by the *re*- or *si*-facial attack to the methyl benzoylformate ketone group, only one methyl mandelate

(26) Zhu, X. Q.; Li, H. R.; Li, Q.; Ai, T.; Lu, J. Y.; Yang, Y.; Cheng, J. P. *Chem. Eur. J.* **2003**, *9*, 871–880.
(27) Simon, L.; Goodman, J. M. *J. Am. Chem. Soc.* **2008**, *130*, 8741–8747.

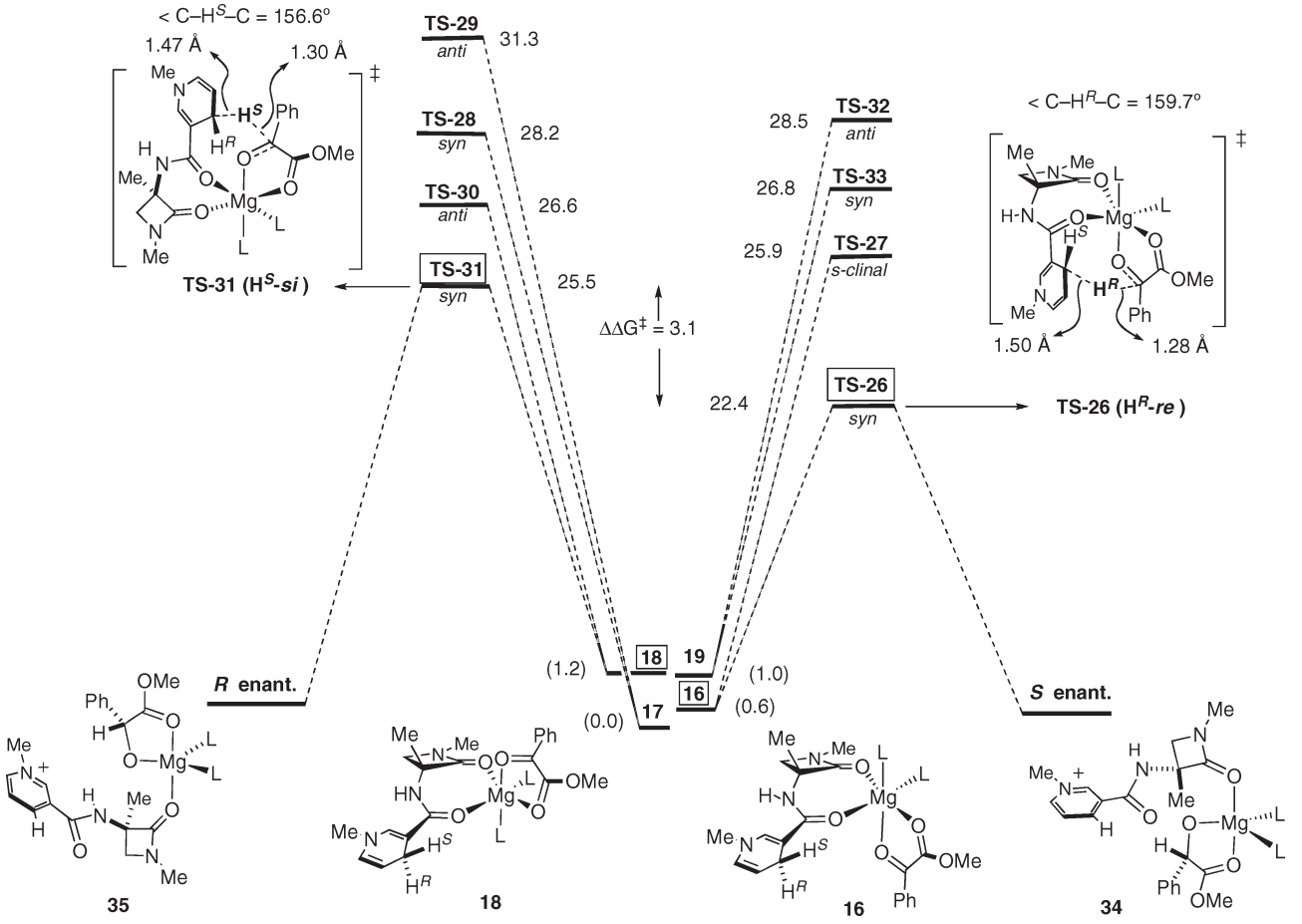

FIGURE 4. Energy diagram ($\Delta G^{\ddagger}$) for the 8 computed pathways (TS-**26**/**33**) of the hydrogen-transfer step in the intramolecular reduction of "productive" ternary complexes **16**−**19** to the (*R*) and (*S*) mandelate complexes. Gibbs energies are in kcal/mol and correspond to the energy differences from the corresponding ternary complexes **16**−**19**. The relative dispositions of the 1,4-dihydronicotinamide C=O and C^2=C^3 bonds are noted as *syn* and *anti*. Some energy levels might not be depicted linearly.

enantiomer could be formed from each ternary complex through two concurrent pathways (Figure 4).

Surprisingly, a reduction in the coordination number at Mg^{2+} from 6 to 5 was observed for the product adducts **34** and **35**. Transformation of the ketone group into an alkoxide anion triggered a change from the octahedral to the trigonal bipyramidal geometry by loosening the coordination with the *N*-methylnicotinium amide carbonyl group. A similar observation has been documented recently on Mg^{2+} ion hexahydrate upon deprotonation of one of the ligands to form the hydroxide anion.[24] The energies of **34** and **35** were 2.9 and 6.6 kcal/mol less stable than their respective starting ternary complexes **16** and **18**. We attributed this discrepancy to a possible inadequate computation "in vacuo" of the charge redistribution from the Mg^{2+} center to the pyridinium salt and magnesium (mono)alkoxide. An inspection of the relative activation enthalpies and Gibbs free energies revealed that transition state TS-**26** (entry 1) represents the lower energy pathway to the (*S*)-methyl mandelate **10**, the main stereoisomer obtained experimentally from the β-lactam NADH peptidomimetics **8** and **5a**−**f**. Transition state TS-**31** (entry 6 in Table 3) was the next most stable and provided the most favorable pathway to (*R*)-methyl mandelate. Both activation energies were in the range $\Delta G^{\ddagger} \approx 22.4$−25.5 kcal/mol, consistent with the experimental reaction conditions (>0 °C) required for the reaction to occur at a measurable rate. They also were in excellent agreement with the values ($\Delta G^{\ddagger} \approx 21$ kcal/mol) reported for related transformations in enzyme-promoted systems.[11c] However, a slight overestimation inherent to the computational method used was noticed for the activation energy difference between the transition states TS-**26** and TS-**31** ($\Delta\Delta G^{\ddagger} \approx 3.1$ kcal/mol) with respect to the ee values (73−90%) measured experimentally for the best silylated β-lactam NADH models **5a**−**f**. Finally, introduction of the solvent factor with the IEF-PCM solvation model (MeCN, $\varepsilon = 36.64$) and carrying out single-point calculations at the B3LYP/6-311++G** level confirmed the activation energy difference ($\Delta\Delta G^{\ddagger} \approx 3.7$ kcal/mol) between the transition states TS-**26** and TS-**31** and validated the values calculated in vacuo at the B3LYP/6-31G* level.

As outlined earlier, ongoing models to explain the facial discrimination of nonenzymatic NADH/Mg^{2+}/PhCO-CO_2Me systems rely on structural observations (e.g., the "H*syn* rule") which are ovserved in free NADH models or, in some cases, on model NADH/Mg^{2+} secondary systems. The translation of such information to the corresponding ternary complexes and transition states is, at least, not obvious. Indeed, we have observed that activation energies calculated either from each individual complex **16**−**19** or from the most stable "productive" ternary complex **17** ($\Delta G^{\ddagger}$ values are

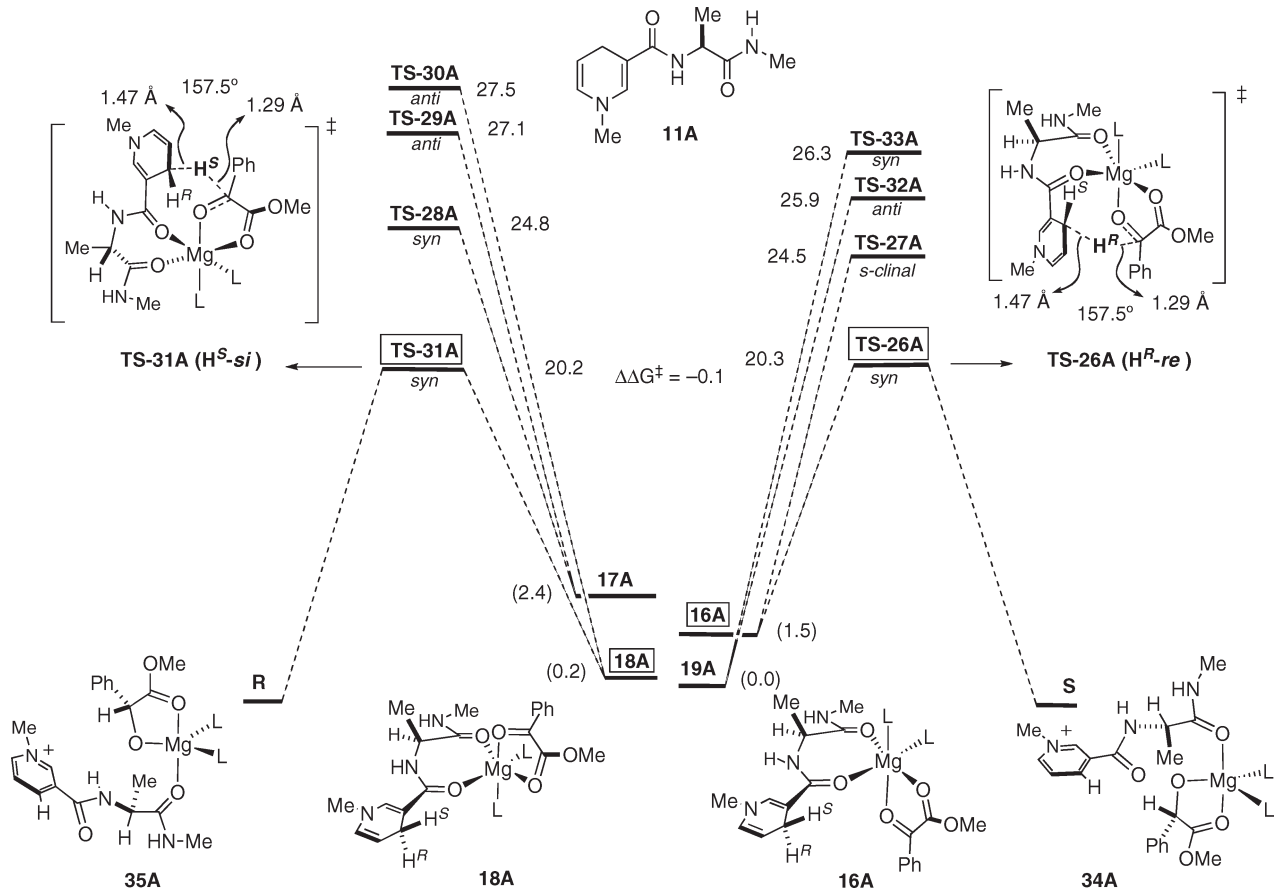

FIGURE 5. Energy diagram ($\Delta G^{\ddagger}$) for the 8 lower activation-energy pathways, using NADH-Ala-NHMe mimetic **11A**. Gibbs energies are in kcal/mol and correspond to the energy differences from the corresponding ternary complexes **16A**−**19A**. Some energy levels might not be depicted linearly.

shown in parentheses in Table 3) were essentially identical. This suggested that the relative stabilities of the different productive ternary structures in the ground state play only a limited role in determining the *R*/*S* configuration of the final products, whereas the relative stabilities of the transition states have a striking importance.

To gain insight into the *structural* origins of the activation energy differences observed for the transition states TS-**26**−**33**, we carefully examined the correlation of $\Delta G^{\ddagger}$ with the torsion angles α, ϕ, and ψ. As shown in Table 3, α torsion angles varied over a wide range depending on the conformation adopted by the 1,4-dihydronicotinamide group around the C^3-C^4 bond to favor the attack of the H^R or the H^S diastereotopic protons to the ketone prochiral face of methyl benzoylformate **9**. In all instances the *syn* conformations ($\alpha \approx \pm 20°$; entries 1, 3, 6, and 8) were preferred over the *synclinal* ($\alpha \approx \pm 45/90$) or *anticlinal* ($\alpha \approx \pm 130/160$) conformations, which were destabilized by up to 3.5 kcal/mol because of the disruption of O=C−C=C $\pi-\pi$ conjugation. These results agreed with previous calculations conducted on model NADH molecules in the ground state,[13g] but raised the question about the suitability of the "H*syn* rule" alone to explain the actual origin of the enantioselectivity observed in enzymomimetic reductions with NADH models. In fact, both transition states *syn*-TS-**26** ($\alpha = 23.1°$) and *syn*-TS-**31** ($\alpha = -20.9°$) obey the rule, but each of them leads to the opposite methyl mandelate enantiomer.

To understand why one particular *syn* transition state structure is more stable than another one, we turned our attention to the torsion angles ϕ and ψ, embodying the strain of the seven-membered chelation ring. In particular, ϕ remained practically unchanged for *syn*-TS-**26** ($\phi = 62.0°$) with respect to the starting ternary complexes **16** ($\phi = 62.1°$) and **18** ($\phi = 67.3°$), but adopted a quite different value for *syn*-TS-**31** ($\phi = -10.7°$). A comparison of the breaking and forming C−H bond lengths within the hydride transfer trajectory also confirmed such differences, yielding a slightly more reagent-like structure for the transition state TS-**31** (Figure 4).

Seeking a confirmation of the foregoing observations, we conducted further computational calculations under identical conditions as before, but using the nonlactamic NADH peptide model **11A**[28] instead of **11** (Figure 5).

The results listed in Table 3 (entries 9−16) revealed two nearly isoenergetic *syn* transition states, TS-**26A** and TS-**31A**, as the pathways of choice to the corresponding (*S*)- and (*R*)-methyl mandelates. Their ϕ dihedral angles were now very similar in absolute value (62.0° and −79.6°, respectively) to those of their corresponding ternary complexes (**16A**, $\phi = 73.4°$; **18A**, $\phi = -80.4°$). Again, the final adducts **34A** and **35A** showed trigonal bipyramidal

(28) To facilitate comparison, we assigned the notation **nnA** to all the ternary complexes and transition states resulting from the replacement of the β-lactam **11** by the open NADH model **11A**.

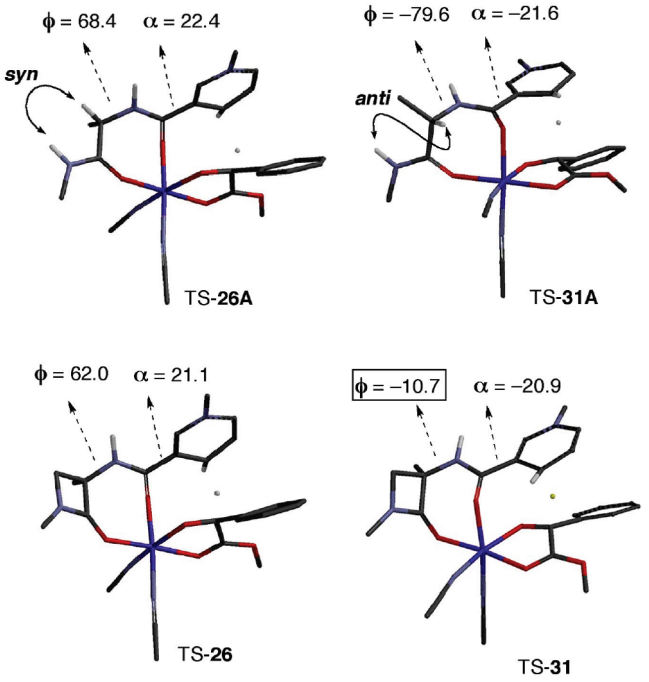

FIGURE 6. Comparison of B3LYP/6-31G*-optimized lower energy transition states TS-**26A** and TS-**31A** (top) with their β-lactam homologues TS-**26** and TS-**31** (bottom). Formal insertion of a methylene bridge (Cα−H + H−N → Cα−CH_2−N) causes the puckering of the chelation pseudoplane in TS-**31**, but not in TS-**26**. All hydrogen atoms except the amide NH, CαH, and NADH C^4H were omitted for clarity.

geometry and the lengths of C−H bonds being cleaved or formed in TS-**26A** and TS-**31A** were also identical in both transition states. Likewise, the torsion angle ψ remained practically constant (≈130°) in either ternary complexes or transition states, and presumably had no influence on the stereochemical outcome of the reaction.

According to the aforementioned computational results, our modeling indicats the formation of quasiracemic mixtures of enantiomers from flexible NADH peptide models. In line with this prediction, Saito and Inoue[7] described recently that 1,4-dihydronicotinamide pseudopeptides containing an (L)-α-amino ester residue reduce methyl benzoylformate **9** in enantiomeric excesses below 23% at room temperature. They noted that the *R*/*S* configuration of the major methyl mandelate depends on the side chain of the (L)-α-amino acid employed and also on the reaction temperature. The conformational changes that, obviously, were suspected to be responsible for such switching[17a] of the chirality of the products can now be rationally understood on the basis of our chelation model.

Finally, comparison of the lower energy transition states arising from the flexible NADH peptide model **11A** and the rigidified NADH β-lactam model **11** (Figure 6) reinforced the idea that a *syn* disposition of the 1,4-dihydronicotinamide $C^2{=}C^3{-}C^4{-}N^5$ bonds ($\alpha \approx \pm 20°$) was necessary but not sufficient to fully explain the stereochemical behavior of NADH/Mg^{2+}/$PhCOCO_2Me$ systems. An additional strain energy caused by the deformation of the seven-membered chelation ring to attain the different transition states from the ternary complexes was found to be the actual reason of the stereodiscrimination in NADH peptide mimetics. Such a strain effect was best viewed by considering the β-lactam transition states TS-**26** and TS-**31** as the result of the formal insertion of a methylene bridge (Cα−H + H−N → Cα−CH_2−N) into the transitions states TS-**26A** and TS-**31A**, respectively. Since the Cα−H and N−H protons of TS-**26A** have a *syn* disposition, their blockage to form a β-lactam ring ($\psi \approx 120°$) caused little change of the central dihedral angle ϕ and, consequently, no extra strain tension in TS-**26**. In contrast, the *anticlinal* disposition of the Cα−H and N−H protons of TS-**31A** provoked a destabilizing puckering of the chelation pseudoplane in TS-**31**, as evidenced by the dramatic change in the torsion angle ϕ.

SCHEME 2. Formation of Binary Complexes of 10 mM Methyl Benzoylformate 9 with Magnesium Perchlorate in Deuterated Acetonitrile

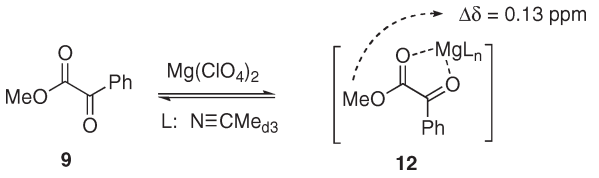

NMR. A series of NMR studies, including chemical shift changes, NOE, and diffusion experiments, were performed next to study the complexation of magnesium perchlorate with methyl benzoylformate **9**, with NADH models **5b** and **5e**, and with combinations of the two. Neither ^{1}H NMR nor ^{13}C NMR spectra of methyl benzoylformate **9** showed perceptible chemical shift changes after the addition of 1 equiv of $Mg(ClO_4)_2$ at room temperature in deuterated acetonitrile (Scheme 2). Only a small downfield shift (0.13 ppm) for the OMe group ^{13}C signal was observed which, in line with our calculations and previous observations,[29] confirmed the weak intensity of the interaction of **9** with the Mg^{2+} cation. DOSY experiments conducted at 20 °C also confirmed these observations and afforded very similar diffusion coefficients (2.50×10^{-9} m^2/s for **9** and 2.35×10^{-9} m^2/s for the binary complex **9**/Mg^{2+}).

We next examined the binary complexes **5b**/Mg^{2+} and **5e**/Mg^{2+}. The conformation of the bis(trimethylsilyl)methyl moiety in NADH models **5b** and **5e** was dramatically affected by the absence or presence of a β-substituent in the azetidinone ring (Figure 7). As previously established in our laboratory using X-ray and NMR techniques,[30] the more stable conformer of β-unsubstituted β-lactams (e.g., **5b**) has a marked preference for a *syn* disposition of the $CH(SiMe_3)_2$ methine C−H bond and the β-lactam carbonyl, whereas the β-substituted analogues (e.g., **5e**) adopt an *anti* relative disposition, resulting in an inversion of the preference of the *pro-R* and *pro-S* $SiMe_3$ groups placed above and below the azetidin-2-one ring plane, respectively.

The ^{1}H NMR spectrum of the binary complex **5b**/Mg^{2+} recorded at room temperature (Figure 7A) was more complicated than expected and showed two sets of signals and four trimethylsilyl groups in the aliphatic region comprised between 1 and −1 ppm. This NMR signal splitting was attributed to the existence of an equilibrium between the chelated conformers **36** and **37** (Figure 7), generated by the

(29) Hoshide, F.; Baba, N.; Oda, J.; Inouye, Y. *Agric. Biol. Chem.* **1983**, *47*, 2141–2143.
(30) Palomo, C.; Aizpurua, J. M.; Benito, A.; Cuerdo, L.; Fratila, R. M.; Miranda, J. I.; Linden, A. *J. Org. Chem.* **2006**, *71*, 6368–6373.

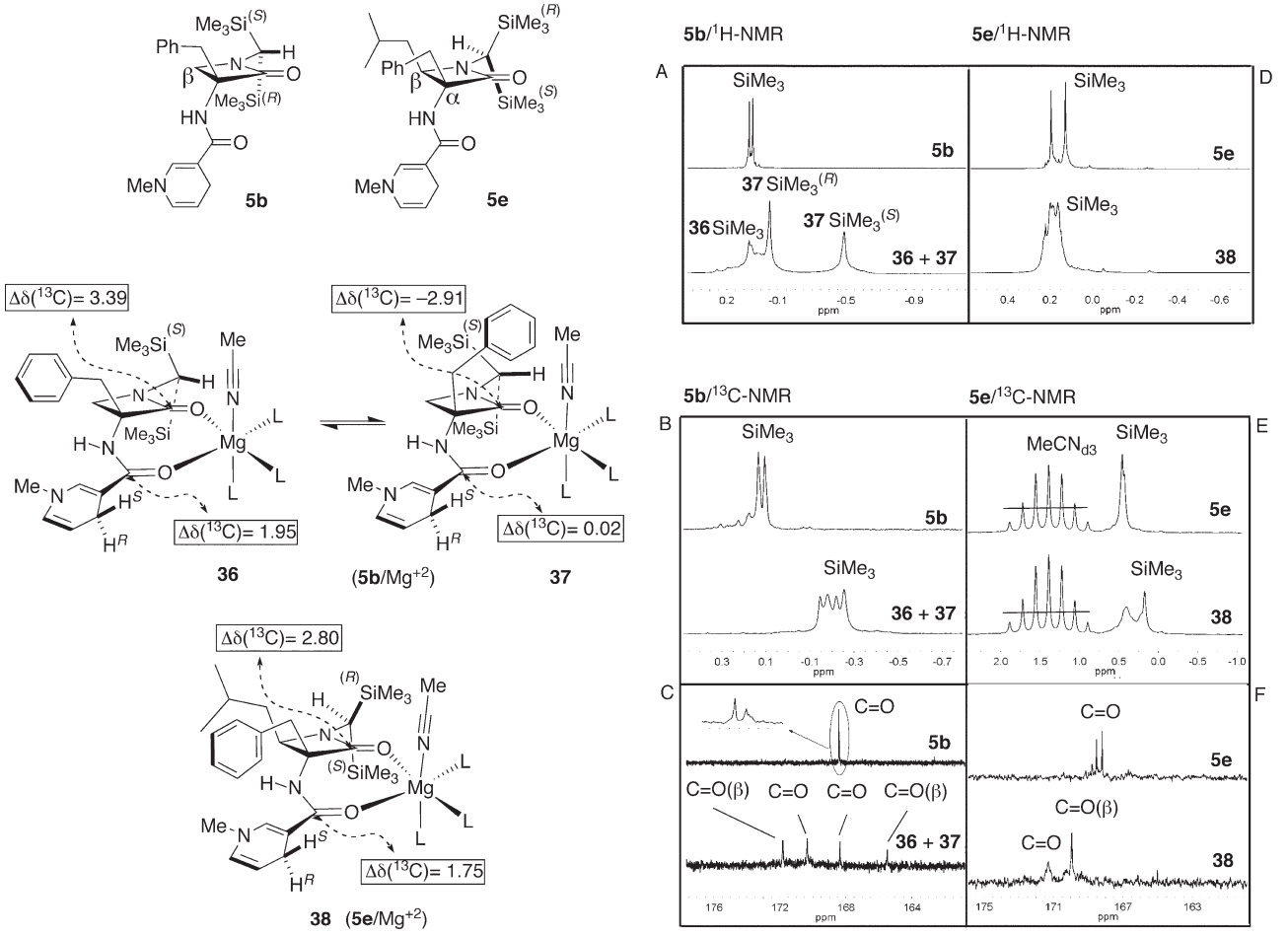

FIGURE 7. Binary complexes of β-lactam NADH peptide models **5b** and **5e** with magnesium perchlorate in deuterated acetonitrile. Carbonyl ^{13}C NMR chemical shift changes (in ppm) for **36**−**38** after the addition of $Mg(ClO_4)_2$ to **5b** and **5e**. Boxes A−F show magnifications of the trimethylsilyl and carbonyl regions of the ^1H NMR spectra (top) and ^{13}C NMR spectra (bottom).

hindered rotation of the benzylic group between the bulky *pro-S* $SiMe_3$ group and the axial acetonitrile ligand. Actually, a total $SiMe_3$ signal coalescence was observed for **36** and **37** above 50 °C and the two sets of signals were restored after recooling the mixture to 20 °C (see the Supporting Information). Further addition of a second equivalent of magnesium perchlorate to the binary complex **5b**/Mg^{2+} resulted in a reunification of the $SiMe_3$ signals into two close singlets, which was interpreted as a rupture of complexes **36** and **37** to form a **5b**/$2Mg^{2+}$ nonchelated species (spectra not shown).

Chemical shift changes in the ^1H NMR and ^{13}C NMR spectra caused by the immobilization of the phenyl group in **37** provided additional information to confirm its structure. First, a selective and large diamagnetic aromatic shielding (−0.55 ppm) of the *pro-S* $SiMe_3$ group distinguished it from the diastereotopic *pro-R* $SiMe_3$ in the ^1H NMR spectrum (Figure 7A). Second, the mixture of complexed conformers **36** + **37** displayed four $SiMe_3$ groups in the ^{13}C NMR spectrum (Figure 7B), resonating between −0.2 and −0.3 ppm upfield from the signals of the free NADH model **5b**. Finally (Figure 7C), the carbonyl carbons of the dihydronicotinamide and the β-lactam shifted 1.95 and 3.39 ppm downfield, respectively, upon complexation to **36**,[31] whereas formation of **37** provoked an upfield shift of −2.91 ppm of the β-lactam carbonyl carbon.

Owing to the spatial disposition of the $CH(SiMe_3)_2$ moiety in the β-substituted NADH model **5e**, it was unlikely that the complex **5e**/Mg^{2+} could adopt a conformation similar to that of **37** with the benzyl group arranged between the *pro-R* $SiMe_3$ group and the axial acetonitrile ligand. In good agreement with this prediction, we observed no diamagnetic upfield shift for $SiMe_3$ signals in the ^1H NMR spectrum of the binary complex **5e**/Mg^{2+} (Figure 7D), and only two signals for $SiMe_3$ and C=O groups in the ^{13}C NMR spectra (Figure 7E,F). Taking into account these observations, we assigned the structure **38** to the complex **5e**/Mg^{2+}.

Next, we examined the interaction of methyl benzoylformate **9** with β-lactam NADH/Mg^{2+} binary complexes. Because of the large separation of the chemical shift observed for $SiMe_3$ groups in complex **37**, the NADH model **5b** was considered to provide the best NMR tagging and was selected for our observations. Experiments were performed with an equimolar mixture of **5b**/$Mg(ClO_4)_2$/**9** in CD_3CN at −40 °C in order to slow down the reduction reaction of **9** to (*S*)-methyl mandelate and

(31) For similar observations on other NADH models, see: Marchelli, R.; Dradi, E.; Dossena, A.; Casnati, G. *Tetrahedron* **1982**, *38*, 2061–2067.

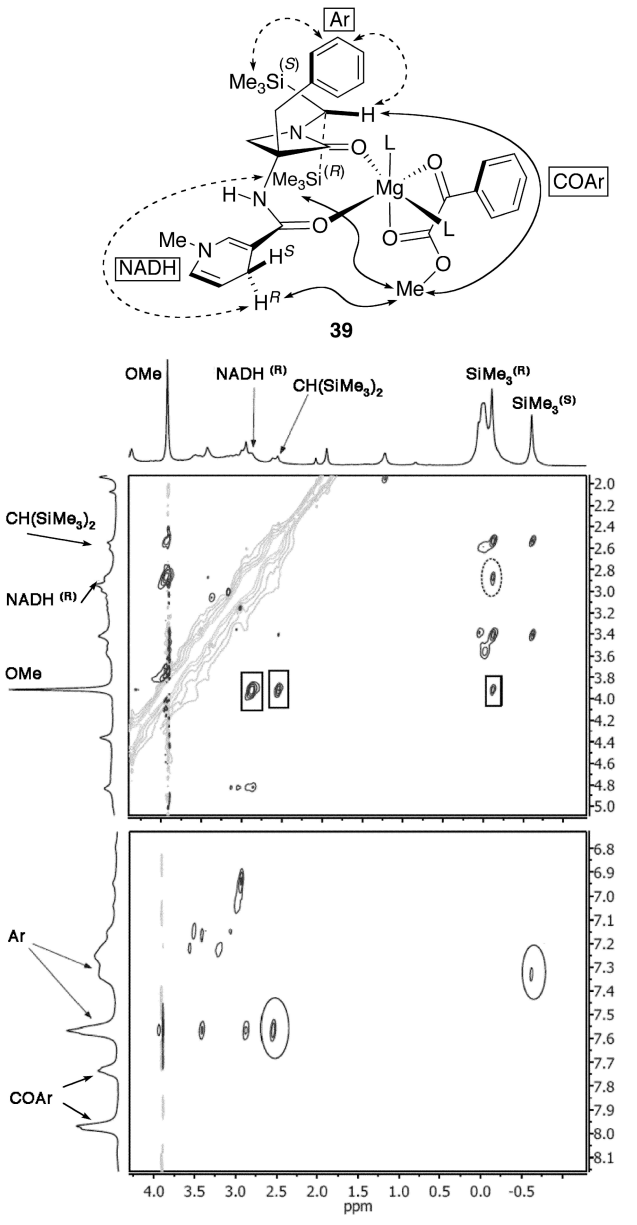

FIGURE 8. Selected extensions of the ROESY spectrum (500 MHz, 400 ms, CD_3CN, −40 °C) of the ternary complex **39** (**5b**/Mg^{2+}/$PhCOCO_2Me$). Intramolecular NOE's correspond to dashed arrows and are inside ellipses; intermolecular NOE interactions are indicated with plain arrows and cross-peaks inside rectangles.

to prevent the decomposition of the NADH mimic. The coexistence of two sets of signals in the ^1H spectrum, one constituted of broad signals and another of sharper peaks, strongly suggested that the "ternary entity" **5b**/Mg^{2+}/**9** was actually formed by an equilibrium of various ternary complexes exchanging the methyl benzoylformate ligand **9** at different rates, in agreement with the conformational complexity predicted by DFT calculations. In addition, the ^{13}C chemical shifts of the NADH carbonyls resonated at intermediate frequencies between the free **5b** and binary complex **5b**/Mg^{2+}, consistent with the formation of a new entity. These data were also supported by the changes observed for the chemical shifts of the dihydropyridine protons in the presence of magnesium perchlorate and **9**. A careful examination of both ^{13}C and ^1H NMR spectra showed that the most significant changes after the addition of 1 equiv of methyl benzoylformate to the binary complex **5b**/Mg^{2+} were suffered by the two diastereotopic $SiMe_3$ groups belonging to the set of "sharp peaks". Finally, measurement of the diffusion coefficient of NADH model **5b** from DOSY experiments showed a significant change from free **5b** (1.42×10^{-9} m^2/s) to the binary mixture **5b**/Mg^{2+} (0.99×10^{-9} m^2/s), but only a very small change was observed upon addition of **9** (1.10×10^{-9} m^2/s). The value of the diffusion coefficient of the methyl benzoylformate in the ternary complex was of 2.62×10^{-9} m^2/s, again very similar to the values observed for the free **9** and binary **9**/Mg^{2+}.

ROESY experiments proved to be particularly helpful to unravel the structure of one of the components of the **5b**/Mg^{2+}/**9** ternary system, which was finally assigned to the complex **39** (Figure 8). Significant "intramolecular" NOE interactions within the NADH model **5b** (indicated with dashed arrows and elipses) and "intermolecular" NOE between **5b** and the methyl benzoylformate ligand **9** (drawn with plain arrows and squares) are detailed in Figure 8. Two key intramolecular cross-peaks were observed for the benzyl aromatic protons (Ar): one with the $CH(SiMe_3)_2$ methyne and another with the *pro-S* $SiMe_3$ group, in good agreement with the previous chemical shift shielding observed for such a group in the binary complex **37** (see Figure 7A). In contrast, the *pro-R* $SiMe_3$ group showed no NOE with the benzyl aromatic protons (Ar) but, instead, a cross-peak with a signal at 2.88 ppm (dotted ellipse) that corresponded to the dihydropyridine H^R proton. On the other hand, three significant intermolecular NOE signals between the OMe group of methyl benzoylformate **9** and the NADH model **5b** were also detected: a first one with the dihydropyridine H^R proton, another one with the $CH(SiMe_3)_2$ methyne proton, and, finally, a third one with the *pro-R* $SiMe_3$ group placed below the chelation pseudoplane.

The above results were in good agreement with the initial computational studies conducted from NADH binary complex model **15** (Figure 3), which anticipated the formation of two sets of ternary complexes, "productive" and "nonproductive", with methyl benzoylformate **9**. In the latter category, the ternary complex **21** with ligand **9** placed in the rear bottom-quadrant position was predicted to be the more stable. Complex **39** showed exactly the same ligand disposition as **21** and its enhanced stability would explain the unusual observation of the "intermolecular" NOE cross-peak signals between **5b** and **9**. Indeed, such signals were not observed or were extremely weak for the "broad" set of peaks arising from **5b**, likely because of the lower stability of the "productive" ternary complex entities. Finally, the ternary complex formed by **9** with the α,β-disubstituted β-lactam model **5e** also failed to provide "intermolecular" NOE cross-peaks, and only the signals corresponding to the binary complex **38** (Figure 7) were recorded. Again, this observation was consistent with the proposed model, since the disposition of both $SiMe_3$ groups in **38**, pointing toward the β-lactam carbonyl, would hinder the placement of the methyl benzoylformate ligand in the rear bottom-half quadrant of the ternary complex.

Conclusions

Strongly rigidified β-lactam peptidomimetic NADH models have been used to investigate the ternary entities NADH/Mg^{2+}/$PhCOCO_2Me$ taking part in the biomimetic reduction of methyl benzoylfomate. According to computational calculations at the B3LYP/6-31G* level, up to 10 stable ternary complexes can be formed by the accommodation of an *s-cis*-methyl benzoylformate ligand around a seven-membered chelation pseudoplane encompassing the Mg^{2+} cation, the β-lactam carbonyl, and the dihydronicotinamide carbonyl. Calculations have also allowed an unambiguous identification of the "productive" ternary complexes, as well as the corresponding transition states leading to the (*S*)- and (*R*)-methyl mandelates with activation energy differences about 3−4 kcal/mol. A comparison of the preferred transition states of the rigidified NADH β-lactam model **11** and the flexible peptide counterpart **11A** has shown that a combination of two conformational features is necessary to attain efficient stereodifferentiation: first, the *syn* disposition of the 1,4-dihydronicotinamide $C^2{=}C^3{-}C^4{-}N^5$ bonds ($\alpha \approx \pm 20°$) to reach the H^R-*re* and H^S-*si* topologies and, second, the diastereomeric deformation of the chelation pseudoplane by blockage of the torsion angles ϕ and ψ to bring the dihydropyridine group from a quasiequatorial disposition in the ternary complexes to a quasiaxial one in the transition structures.

In agreement with theory, some α,β-substituted β-lactam NADH mimetics synthesized yielded the expected (*S*)-methyl mandelate enantiomer in up to 90% ee, albeit calculated $\Delta\Delta G^{\ddagger}$ values suggested higher enantiomeric excesses. Furthermore, it has been shown that two diastereotopic trimethylsilyl groups incorporated close to the β-lactam ring can act as NMR-tags. This has permitted the identification of the structure of an exceptionally stable "nonproductive" ternary complex and its structural determination by ROESY experiments including for the first time cross-peak signals between an NADH model and methyl benzoylformate. Studies concerning the extension of the proposed model to the realm of monodentate NADH mimetics and to different carbonyl substrates are currently underway in our laboratory.

Experimental Section

General Procedure for the Preparation of 3-Alkyl-1-[bis-(trimethylsilyl)methyl]-3-nicotinamidoazetidin-2-ones 7a−f. To a solution of the nicotinoyl chloride hydrochloride (3.6 mmol, 0.64 g) in 40 mL of dry CH_3CN cooled to −5 °C under nitrogen atmosphere were added *N*,*N*-diisopropylethylamine (DIPEA) (24 mmol, 4.2 mL) and a solution of the corresponding α-amino-β-lactam (3 mmol) in 10 mL of CH_3CN. The reaction mixture was stirred for 1 h at 0 °C, then at room temperature (5 to 18 h, monitored by ^{1}H NMR). After that time, CH_2Cl_2 (20 mL) was added and the solution was washed with 0.1 M NaOH (20 mL), NH_4Cl (20 mL), and H_2O (20 mL). The organic phase was decanted and dried over $MgSO_4$. The solvents were evaporated under reduced pressure and the crude extract was purified by flash chromatography (eluent: EtOAc).

General Procedure for the Preparation of *N*-Methyl-1,4-dihydronicotinamides 5a−f. To a solution of the corresponding nicotinamide **7** (0.5 mmol) in CH_3CN (5 mL) under N_2 atmosphere was added methyl iodide (3 mL). The reaction mixture was stirred at 50 °C for 2−24 h. After that time, the solvents were evaporated and the residue was dried under vacuum to afford the pyridinium iodide as a hygroscopic solid that was used without further purification. To a solution of the corresponding pyridinium salt (0.5 mmol) in 12 mL of deoxygenated CH_2Cl_2/MeOH (3/1) was added a deoxygenated solution of $Na_2S_2O_4$ (10.0 mmol) in 0.5 M aqueous Na_2CO_3 (12.5 mL) and the mixture was vigorously stirred under nitrogen in the dark for 16 h (the color of the solution quickly turned from orange to yellow). The organic layer was separated, the aqueous phase was extracted with CH_2Cl_2 (deoxygenated; 2 × 10 mL), and the combined organic phase was dried ($MgSO_4$) and concentrated in vacuo to give the crude corresponding dihydropyridine, which was used in the following reaction without further purification. These compounds can be kept for 24−48 h at −30 °C without oxidation or decomposition.

General Procedure for the Biomimetic Reduction of Methyl Benzoylformate with the NADH Models 5a−f and 8. All reactions were conducted in the dark, under a nitrogen atmosphere, at room temperature, in sealed NMR tubes or flasks. In a typical run, a solution of the NADH model (0.103 mmol, 1.1 equiv), $Mg(ClO_4)_2$ (0.103 mmol, 1.1 eq., 23.0 mg), and methyl benzoylformate (0.093 mmol) in 0.7 mL of deoxygenated CD_3CN was prepared in a dried NMR tube in the dark and the reaction was followed by ^{1}H NMR. After complete consumption of the NADH model, H_2O was added and the aqueous layer was extracted with CH_2Cl_2 (4 × 2 mL). The combined organic layers were dried over $MgSO_4$ and the solvent was evaporated under reduced pressure. The crude reaction mixture was submitted to HPLC analysis although in some cases the resulting mandelate was isolated by preparative thin layer chromatography (eluent: hexanes/EtOAc). Enantiomeric excesses were determined by HPLC, using chiral stationary phases (Chiralcel OD) and hexanes/isopropanol as the mobile phase. Detailed reaction conditions, yields, and HPLC conditions are provided in the Supporting Information (Table S1).

Acknowledgment. We thank the Ministerio de Educación y Ciencia (MEC, Spain) (Project: CTQ2006-13891/BQU), UPV-EHU, and Gobierno Vasco (ETORTEK inanoGUNE IE-08/225) for financial support. Thanks are also due to SGI/IZO-SGIker for the generous allocation of computational resources and to SGIker (UPV/EHU) for NMR facilities. A grant from Gobierno Vasco to R.M.F. is acknowledged.

Supporting Information Available: Preparation procedures, physical and spectroscopic data for compounds **5a−f**, **7a−f**, and **8**, HPLC chromatograms for ee determination, NMR spectra of complexation and diffusion studies, Cartesian coordinates of all computed stationary points, relative and absolute activation energies for all reactions, and complete ref 22. This material is available free of charge via the Internet at http://pubs.acs.org.